**48º CONGRESO ESPAÑOL DE ACÚSTICA
ENCUENTRO IBÉRICO DE ACÚSTICA
EUROPEAN SYMPOSIUM ON UNDERWATER ACOUSTICS
APPLICATIONS
EUROPEAN SYMPOSIUM ON SUSTAINABLE BUILDING
ACOUSTICS**

ULTRASONIC WAVE PROPAGATION SIMULATION TO DETECT CRACKS IN CONCRETE STRUCTURES USING FEM

Carlos Albino[1], Luís Godinho[1], Daniel Dias-da-Costa[2,1], Delfim Soares Jr.[3]
[1]ISISE, Departamento de Engenharia Civil, Universidade de Coimbra,
Rua Luís Reis Santos - Pólo II da Universidade
3030-788 Coimbra, Portugal
{capa@uc.pt, lgodinho@dec.uc.pt, dias-da-costa@dec.uc.pt}
[2]School of Civil Engineering, The University of Sydney,
NSW 2006, Australia
{daniel.diasdacosta@sydney.edu.au}
[3]Structural Engineering Department, Federal University of Juiz de Fora,
CEP 36036-330, Juiz de Fora, MG, Brazil
{delfim.soares@ufjf.edu.br}

Keywords: Crack detection, Non-destructive testing, Time domain, Wave propagation.

ABSTRACT

Despite the recent technological developments, many techniques available for assessing concrete structures are still based on visual inspections and do not allow the timely detection of damage. In this context, ultrasonic-based methods may have several advantages, particularly in terms of the early stage detection of damage and cracking. In this paper, the propagation of ultrasonic waves inside a cracked concrete structure is analysed. For this purpose, an advanced finite element model formulated in the time domain was developed, which includes the presence of waves P, S and guided waves (e.g., surface waves). The model allows the simulation of the propagation of ultrasonic waves in a structure with the evolution of damage. The obtained results allow a better understanding of the phenomenon involved and, in this way, can contribute to the development of new cracking detection equipment.

RESUMO

Apesar dos desenvolvimentos tecnológicos recentes, muitas técnicas de avaliação de estruturas de betão são ainda baseadas em inspeções visuais que não permitem uma deteção atempada de danos. Neste âmbito, técnicas baseadas em ultrassons podem apresentar várias vantagens, especialmente no que concerne a deteção de dano e de potencial fissuração no seu estágio inicial. Neste artigo, procura-se analisar a propagação deste tipo de ondas no interior de uma estrutura de betão sujeita a fissuração. Para esse efeito, foi desenvolvido um modelo numérico avançado de elementos finitos formulado no domínio do tempo. O modelo permite a simulação da propagação de ondas ultrassónicas numa estrutura com evolução progressiva de dano, sendo considerada a presença de ondas P, S e de ondas guiadas (de superfície, por exemplo). Os resultados apresentados permitem compreender melhor os fenómenos envolvidos e, desta forma, contribuir para o desenvolvimento de novos equipamentos para deteção de fissuração.

48º CONGRESO ESPAÑOL DE ACÚSTICA
ENCUENTRO IBÉRICO DE ACÚSTICA
EUROPEAN SYMPOSIUM ON UNDERWATER ACOUSTICS
APPLICATIONS
EUROPEAN SYMPOSIUM ON SUSTAINABLE BUILDING
ACOUSTICS

INTRODUCTION

Many concrete buildings built in recent times are showing early signs of damage and aging, which are often the result of poor design, inferior quality of materials, and exposure to increasingly aggressive environments [1]. Thus, it is important to intervene to control the progress of degradation and to extend the life span of the structure. The early diagnosis of structural defects is essential to decide and plan effective actions that can mitigate the structural degradation at an acceptable cost. In this scope, the inspection and evaluation of concrete structures is, in most cases, still performed by visual survey methods, with some destructive testing techniques being available to support the analysis, either *in situ* or at the laboratory. In the case of concrete cracking, the diagnosis can be particularly challenging because the cracks are often not visible in the initial phase. However, it is recognised that this stage – i.e. the onset of cracking – is extremely important for early interventions designed to restore the structural performance. The use of non-destructive techniques – such as the ones based on ultrasounds – have shown the potential to detect cracks and even predict their depth.

Ultrasonic techniques are based on the propagation of mechanical waves with frequencies above 20 kHz. The propagation is deeply influenced by the presence of obstacles or discontinuities in the medium, which impact the different travel times observed – particularly in comparison with a sound and homogenous medium [2]. Non-destructive ultrasonic techniques require the use of ultrasonic transducers, and receivers that measure the response time of the pulse generated by a source. Since the presence of cracks and voids will affect the propagation time of the ultrasonic wave, this information can be used to infer the most likely type of damage in the structure. The physical phenomena within the solid propagation medium is, however, quite complex.

When a solid material is excited by mechanical impulses, three different types of waves are generated. The compression waves or primary waves (P) are those with the highest propagation velocity, defined by equation (1). These, are longitudinal waves causing displacements in the medium parallel to the direction of the wave, although they are the least energetic.

$$v_P = \sqrt{\frac{E(1-\nu)}{\rho(1+\nu)(1-2\nu)}} \qquad (1)$$

The shear waves or secondary waves (S) are transverse waves causing displacements in the medium, and they are perpendicular to the direction of the propagation. These waves are slower than the P waves and their speed is defined by:

$$v_S = \sqrt{\frac{E}{2\rho(1+\nu)}} \qquad (2)$$

The surface waves are the slowest. Due to their low frequency, longer duration and larger amplitude, they are the most energetic. There are several types of surface wave – such as Rayleigh and Love waves. They usually are the result of the interference between P and S waves with boundary or interface surfaces, and for the case of Rayleigh waves their velocity is approximated by the following equation:

$$v_R = \frac{0.87 + 1.12\nu}{1+\nu} \sqrt{\frac{E}{2\rho(1+\nu)}} \qquad (3)$$

48º CONGRESO ESPAÑOL DE ACÚSTICA
ENCUENTRO IBÉRICO DE ACÚSTICA
EUROPEAN SYMPOSIUM ON UNDERWATER ACOUSTICS
APPLICATIONS
EUROPEAN SYMPOSIUM ON SUSTAINABLE BUILDING
ACOUSTICS

Rayleigh waves cause elliptical orbit displacements in the medium particles and their amplitude decreases rapidly with the depth.

In the specific case of ultrasonic waves, the presence of the different wave mentioned above leads to complex propagation patterns even in simple medium geometries, which can hinder the clarity of signals and their interpretation. Ultrasound methods are well-known and commonly used in the analysis of defects in steel structures. For example, in crack sizing, techniques based on the time of flight diffraction have been reported as accurate in several works [3-5]. Such techniques employ longitudinal waves which are transmitted and received using contact transducers positioned along the surface. In non-homogeneous materials, such as concrete, the problem becomes more complex, since the heterogeneity of the material can also influence the high-frequency pulses, and lower frequencies may be required [6]

This paper presents the numerical analysis of the propagation of ultrasound waves in a concrete specimen to assess how this is impacted by internal cracks. For this purpose, a numerical model based on the finite element method formulated in the time domain is herein proposed. The time marching algorithm was recently developed by Soares [7] and is adopted to render the numerical process more efficient.

NUMERICAL MODEL

The governing equations of the model and the main aspects related with the time integration strategy are presented. The algorithm is based only on single-step displacement-velocity relations and it requires no system of equations to be dealt with (once lumped mass matrices are considered). It is second-order accurate and allows the dissipation of spurious modes, which makes it very effective and able to provide accurate analyses with relatively large time steps. Moreover, since the algorithm has high stability limits, it minimises the main drawback of explicit procedures, allowing time-steps that are only usual in accurate implicit analyses, rendering good results at reduced computational costs [7, 8]. The equations used for the analysis of the proposed problem, read as follows:

$$\mathbf{E}\dot{\mathbf{U}}^{n+1} = \mathfrak{I}_{\mathbf{F}}^{n+\frac{1}{2}} + \mathbf{M}\dot{\mathbf{U}}^n - \frac{1}{2}\Delta t \mathbf{C}\dot{\mathbf{U}}^n - \mathbf{K}\left(\Delta t \mathbf{U}^n + \frac{1}{2}\Delta t^2 \dot{\mathbf{U}}^n\right) \tag{4}$$

and

$$\mathbf{E}\mathbf{U}^{n+1} = \mathbf{E}\left(\mathbf{U}^n + \frac{1}{2}\Delta t \dot{\mathbf{U}}^n + \frac{1}{2}\Delta t \dot{\mathbf{U}}^{n+1}\right) - \frac{1}{2}\Delta t^2 \mathbf{C}\dot{\mathbf{U}}^{n+1} - \mathbf{K}\left((\beta b_1 b_2)\Delta t^3 \dot{\mathbf{U}}^n + \left(\frac{1}{16} + \beta b_1\right)\Delta t^3 \dot{\mathbf{U}}^{n+1}\right) \tag{5}$$

where $\mathbf{C}$ is the damping matrix, $\mathbf{E} = \mathbf{M} + \frac{1}{2}\Delta t \mathbf{C}$ is the effective matrix, $\mathbf{M}$ and $\mathbf{K}$ stand for the mass and stiffness matrices, respectively; $\mathbf{U}$, $\dot{\mathbf{U}}$ and $\mathbf{F}$ stand for the displacement, velocity and load vectors, respectively; n and Δt are the time-step number and time-step length, respectively; $\beta = 1$, $b_1 = 8.567 \times 10^{-3}$ and $b_2 = 8.590 \times 10^{-1}$ are the time integration parameters of the new method; $\mathfrak{I}_{\mathbf{F}}^{n+1/2} = \beta_1 \Delta t \mathbf{F}^n + \beta_2 \Delta t \mathbf{F}^{n+1}$, with $\beta_1 = \beta_2 = 1/2$, using trapezoidal quadrature rule or $\beta_1 = 1$ and $\beta_2 = 0$, extending the explicit feature of the technique to the load term – see [7] for more details.

48º CONGRESO ESPAÑOL DE ACÚSTICA
ENCUENTRO IBÉRICO DE ACÚSTICA
EUROPEAN SYMPOSIUM ON UNDERWATER ACOUSTICS
APPLICATIONS
EUROPEAN SYMPOSIUM ON SUSTAINABLE BUILDING
ACOUSTICS

NUMERICAL RESULTS

The numerical methodology devised in this work is applied to a single edge notched concrete beam of small size, with maximum aggregate size of 8 mm – see experimental details in [9]. The beam measures $400{\times}100{\times}100$ mm^3 has a $5{\times}20{\times}100$ mm^2 notch, located at the middle of the top as shown in Figure 1 a). The corresponding material parameters are: density ρ = 2500 kg/m^3; Young's modulus E = 35 000 N/mm^2; Poisson's ratio ν = 0.15; tensile strength f_{t0} = 3.0 N/mm^2; and fracture energy G_F = 0.1 N/mm. A constitutive law described in [10] is used, with normal stiffness k_n = 10^5 N/mm^3 and shear stiffness k_s = $4{\times}10^2$ N/mm^3. The crack paths presented in Figure 1 b) as c) are obtained from numerical simulations (see detailed description in [11]) and are in agreement with the experimental crack [10]. After the calculation of the crack pattern for the different stages, the FEM cracked model is used as the geometry input data for the Time Domain FEM model. For the presented test case, three distinct stages are considered (see Figure 1): the initial defect-free beam; the beam in the cracked stage, first with the crack tip at 57 mm and next at 40 mm above the bottom of the beam.
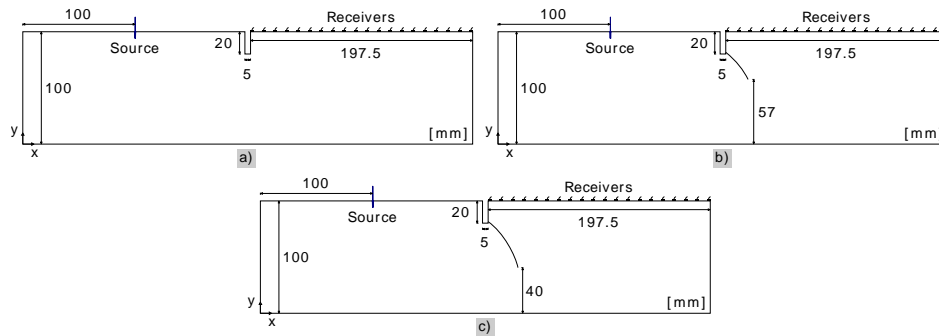
Figure 1 – Schematic representation of the models used for wave propagation analysis: (a) uncracked beam; (b) beam with crack tip at 57 mm above the bottom; (c) beam with crack tip at 40 mm above the bottom.

The system is excited by a Ricker pulse whose source is located at (100, 100) mm. The area to the right of the crack is the area of interest for ultrasound signal analysis. Therefore, the response is evaluated at a set of receivers placed along this area. For the reliability of the method, at least 8 elements per wavelength are used to model the structural element.

For each of the proposed cracked beam geometries, a geometric ray analysis may be used to predict the most likely P-P and S-S wave paths for the earlier pulses reaching the receivers. In Figure 2 this geometrical analysis is schematically represented for the longer crack (tip at 40 mm from the bottom), considering two receiver positions, both placed to the right of the crack, at different distances along the X direction; the first is located half-way between the notch and the right end of the beam and the second is located closer to the notch, at a quarter distance between the notch and the right end of the beam. For the first case, the expected first arrivals are originated by the diffraction of the incident wave by the crack tip, and by the back-wall echo effect at the bottom of the beam. These two paths are identified in the Figure 2, respectively as Paths 1 and 2. When the receiver is positioned closer to the notch, the first arrival still corresponds to the pulse diffracted by the crack tip, but some changes occur for the second identified path. In this case, the propagation path is intercepted by the crack, and the diffraction by the crack tip also occurs after the reflection from the back-wall. It can be said that the receiver point is now shadowed by the presence of the crack, and the expected time of flight of this pulse should increase when compared to the uncracked configuration.
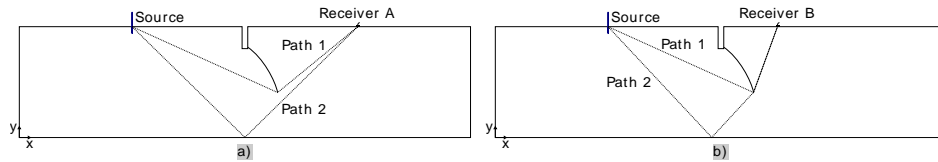
Figure 2 – Illustrative sketch of the waves paths for the first two arrivals expected in the time signals.

The wave propagation velocities considered for this case are 3844.8 m/s for P-waves and 2467.2 m/s for S-waves. Figure 3 illustrates the results calculated for the propagating Ricker pulse with a central frequency of 100 kHz using several damping factors. The scale of the figures is intentionally made different for each situation, such that the most significant pulses can be highlighted. The higher damping factor has an effect of cleaning the weaker pulses, transporting less energy, revealing the path of the most important pulses; in that case, as expected, later arrivals almost disappear, since their energy is progressively dissipated by the material damping.
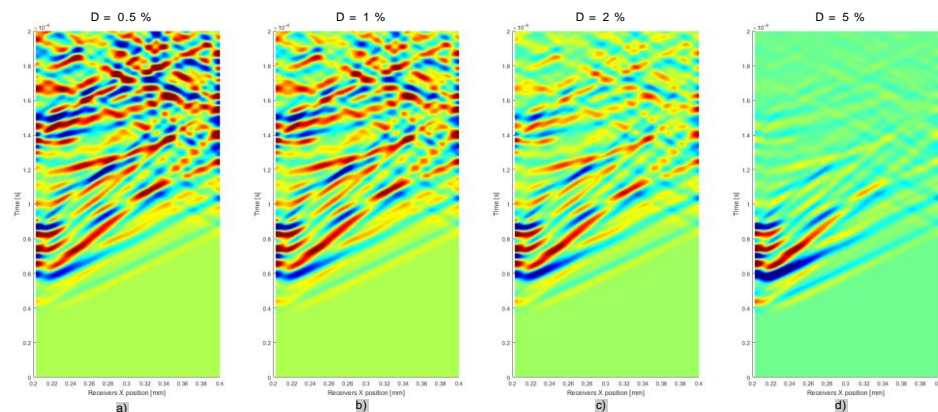
Figure 3 – Time responses determined for the receivers positioned at the top, for the uncracked beam using damping: a) 0.5 %, b) 1 %, c) 2 % and d) 5 %

Figure 4 shows the time signals obtained for two different frequencies of the ultrasonic pulse: 100 kHz and 150 kHz. For both frequencies, it is clear that significant differences in the wave propagation pattern are registered for the two crack lengths. For this purpose, a damping factor of 2 % was used. Comparing plots 1) and 2) it is verified that the arrival of the first wave to the receivers exposes relevant characteristics that can be used to infer the length of the crack. Indeed, this first arrival is generated by the diffraction effect at the crack tip (or at the bottom of the beam) as identified before, which tends to occur later as longer cracks are considered (see schematic representation in Figure 2). This variation in the arrival times is mostly visible at receivers placed closer to the notch (Receiver B). In addition, for longer cracks this diffraction effect originates a stronger deviation in the wave path and thus a lower amount of energy reaches the receivers; this effect is also clearly visible in pictures 1) and 2). In Figure 4 b) 2) the times-of-flight are identified for two receivers that will be later characterised in Figure 6 in more detail.

Figure 5 shows the time signals registered for all stages of the beam: unnotched (perfect beam), a), notched, b), and for the two crack lengths, c) and d). The source emitting the Ricker pulse is located at the same location as before and the receivers are placed along the right-bottom edge of the beam (202.5 – 400.0) mm. It is observed that the arrival of the first wave is not influenced by the notch, nor by the two crack lengths defined in Figure 1. However, next to the notch X position the influence of the reflections of notch and crack is evident. In the lower right corner of the single beam there is a late concentration of energy resulting from the reflections at the boundaries of the beam, as shown in the upper right corner of Figure 5 a).
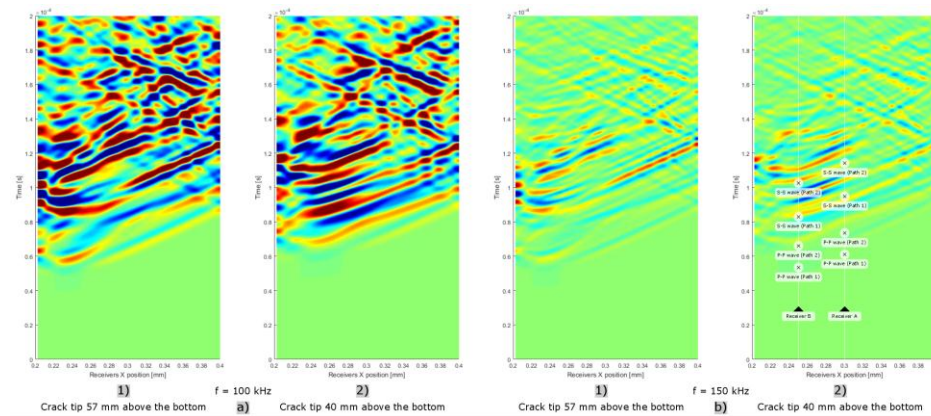
Figure 4 – Time responses determined for the receivers positioned at the top of the beam, for the cracked beam with crack tip at 1) 57 mm and 2) 40 mm above the bottom, for frequencies a) 100 kHz and b) 150 kHz
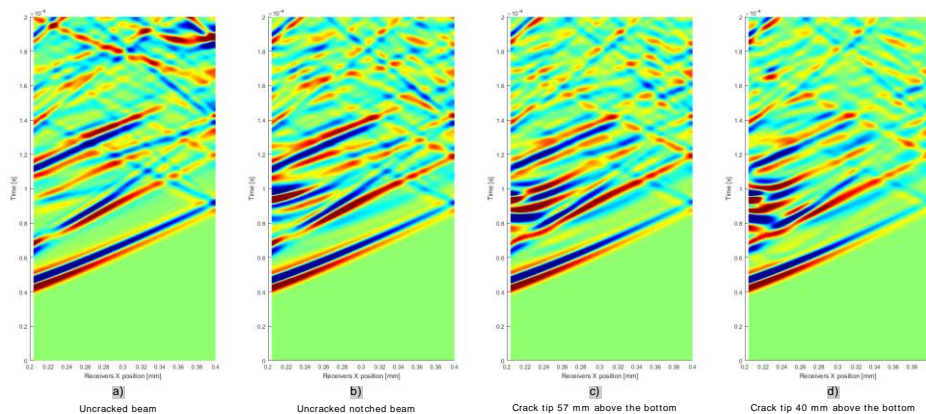
Figure 5 – Time responses determined for the receivers positioned at the bottom of the beam, for the a) uncracked and unnotched beam, b) uncracked and notched beam, c) cracked beam with crack tip at 57 mm above the bottom and d) cracked beam with crack tip 40 mm above the bottom

To have a more detailed insight of the presented results, analyses of two individual receiver positions (A at (300,100) mm and B at (250,100) mm) – see representation in Figure 2 – are performed for the model with the longer crack path (Figure 1) by focusing on the expected arrival times of the earlier arriving pulses. For each receiver, it is possible to compute the time-of-flight

48º CONGRESO ESPAÑOL DE ACÚSTICA
ENCUENTRO IBÉRICO DE ACÚSTICA
EUROPEAN SYMPOSIUM ON UNDERWATER ACOUSTICS
APPLICATIONS
EUROPEAN SYMPOSIUM ON SUSTAINABLE BUILDING
ACOUSTICS

(TOF) of the two paths identified in Figure 2, using a geometrical ray analysis (see **¡Error! No se encuentra el origen de la referencia.**). As expected, for each receiver and for each path, the first pulses are related to the P-P waves. For receiver A, the crack does not interfere with Path 2.

Table 1 – Time-of-flight of receivers A and B

Time-of-flight	Receiver A		Receiver B	
[ms]	Path 1	Path 2	Path 1	Path 2
P-P Waves	0.06100	0.07356	0.05331	0.06602
S-S Waves	0.09506	0.11464	0.08308	0.10288

In Figure 6, two plots illustrate detailed views of the calculated time responses at the two receivers, for both cracked and uncracked beams, together with the estimated arrival times of the first two pulses induced by P-P and S-S waves, corresponding to Paths 1 and 2. The presented results were calculated for an ultrasonic frequency of 150 kHz (with a P-wave wavelength of 25.6 mm and a S-wave wavelength of 16.4 mm) and with a damping factor of 3 %.

Observing the response computed for receiver A in Figure 6 a), it is possible to identify the marked delay that occurs in the arrival times of the first pulse when the cracked beam is considered; this delay is directly related to the longer path that the P-P waves need to travel due to the presence of the crack. It may also be noted that the arrival time for this first pulse matches perfectly the predicted TOF presented above and identified with a triangular mark. As for the second arrival, the delay is much smaller and less noticeable, but a decrease of amplitude is registered. Later on, the arrival time of S-S waves through path 1 causes an increase in amplitude which is again amplified by the arrival of the same type of waves coming from path 2. Again, the arrival times for this pulses match perfectly the estimated TOF. It is also noted that since Path 2 does not intercept the crack, the arrival time of the second pulse remains unchanged, and theses pulses appear almost overlapped at this receiver; it should be noted that there is not an exact match between the two curves at this point due to the influence of the many other energy paths connecting the source to the receiver. This is most noticeable in the arrival time of S-S waves.
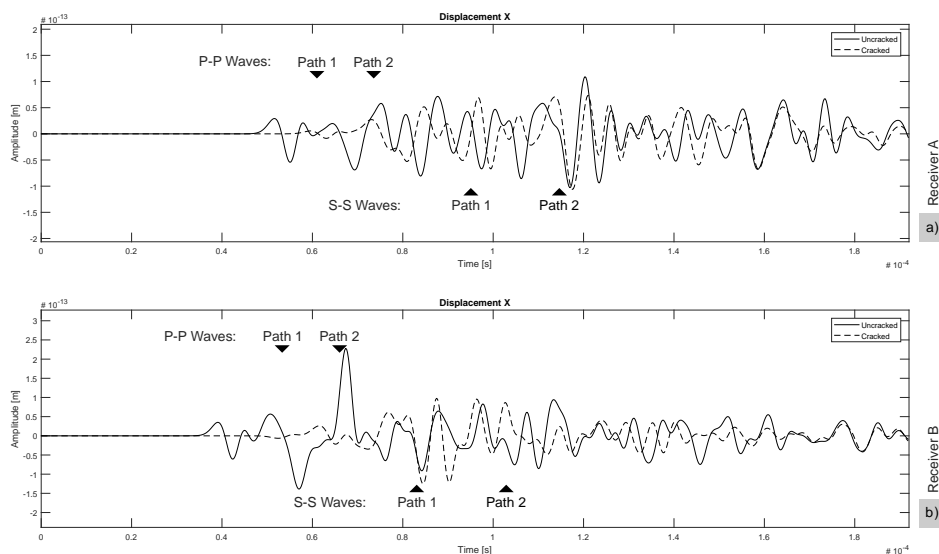
Figure 6 – Responses computed at receivers a) A and b) B, for uncracked and cracked (crack tip 40 mm above the bottom) states. The triangular marks depict the TOF estimated using geometrical ray analysis.

48º CONGRESO ESPAÑOL DE ACÚSTICA
ENCUENTRO IBÉRICO DE ACÚSTICA
EUROPEAN SYMPOSIUM ON UNDERWATER ACOUSTICS
APPLICATIONS
EUROPEAN SYMPOSIUM ON SUSTAINABLE BUILDING
ACOUSTICS

The analysis of receiver B (Figure 6 b)) shows similar features, with a very visible delay being registered for the first arrival of P-P waves. In the second arrival, the delay is much smaller and less noticeable. Indeed, due to the fact that it now corresponds to a diffracted pulse, the energy of the pulse that travels along Path 2 is spread after reaching the crack tip, and thus the pulse is considerably attenuated. As before, the match between the TOF estimated using geometric ray analysis and the arrival times observed in the numerical response are excellent. After the analysis of the plotted results, it is possible to confirm that, for the studied configuration, the delay of the first arrival of P-P waves is the most relevant feature when trying to localise the presence and position of a possible embedded crack.

Given the described results, it may be stated that the P-P and S-S waves propagation patterns within the concrete beam are strongly influenced by the size of the crack, and that the responses registered at the receiver points may be of use for the evaluation of the damage within the beam. It is also important to note that concrete is, typically, a non-homogeneous material, and thus the propagation of high frequency waves may be significantly influenced by the small heterogeneities (e.g. aggregates, small voids, etc.). For this reason, it is common to make use of ultrasonic frequencies between 20 kHz and 150 kHz [6] for real sized concrete elements, or somewhat higher frequencies when small elements are to be analysed.

CONCLUSIONS

In this paper, the authors devised a numerical approach to simulate the process of crack detection in concrete elements using P and S waves based on ultrasound methods. The numerical tool enables the accurate simulation of the propagation of ultrasonic waves in a progressively damaged structure and can be used for detection purposes. The implementation is very efficient, since it uses an innovative time-stepping algorithm. A test case was presented, which allowed to conclude that cracks can be identified by the propagation of P and S waves. The presented results also compared the effects of cracks of different lengths – i.e. corresponding to increasing damaged states – in the time signals registered at receiver points located at the structure surface. Results are promising and show the feasibility of using P and S waves based ultrasonic equipment for on-site applications in the future.

ACKNOWNLEDGEMENTS

REFERENCES

[1] J. Gomes; L. Oliveira; J. Lanzinha; M. Almeida, Técnicas de Inspecção e Avaliação de Estruturas de Betão, 2014.

[2] A. Medeiros, Aplicação do Ultra-Som na Estimativa da Profundidade de Fendas Superficiais e na Avaliação da Eficácia de Injeções em Elementos de Concreto Armado, Dissertação de Mestrado em Engenharia Civil, Universidade Federal de Santa Catarina, Florianópolis, 2007.

[3] Charlesworth JP, Temple JAG. Engineering applications of ultrasonic time-of-flight diffraction. Philadelphia: Research Studies Press; 2001.

[4]   Ogilvy JA, Temple JAG. Diffraction of elastic waves by cracks: application to time-of-flight inspection. Ultrasonics. 1983;21:259-69. Doi: 10.1016/0041-624x(83)90058-6.

[5]   Capineri L, Tattersall HG, Silk MG, Temple JAG. Time-of-flight diffraction tomography for NDT applications. Ultrasonics. 1992;30:275-88. Doi: 10.1016/0041-624x(92)90001-3.

[6]   IAEA. Guidebook on NDT of concrete structures: training course series. International Atomic Energy Agency, No. 17, 242, Vienna; 2002.

[7]   D. Soares, A novel family of explicit time marching techniques for structural dynamics and wave propagation models, Computer Methods in Applied Mechanics and Engineering, 311, 2016, PP 838-855.

[8]   D. Soares, An explicit multi-level time-step algorithm to model the propagation of interacting acoustic-elastic waves using finite element / finite difference coupled procedures, Comput. Model. Eng. Sci. 17 (2007) 19–34.

[9]   Schlangen E. Experimental and numerical analysis of fracture processes in concrete. Delft University of Technology, Delft, the Netherlands; 1993.

[10] Wells GN, Sluys LJ. Three-dimensional embedded discontinuity model for brittle fracture. Int J Solids Struct 2001; 38:897-913. http://dx.doi.org/10.1016/S0020-7683(00)00029-9.

[11] L. Godinho; D. Dias-da-Costa; P. Areias; E. Júlio; D. Soares Jr., Numerical study towards the use of a SH wave ultrasonic-based strategy for crack detection in concrete structures, Engineering Structures, 49, 2013, pp 782-791.